Physical Principles and Equipment of Intravascular Optical Coherence Tomography

10

Jinyong Ha

Optical coherence tomography (OCT) is an emerging imaging modality analogous to intravascular ultrasound imaging but uses light instead of sound. The integration of a fiber-optic probe with frequency domain OCT enables video images that display the location and changes of coronary plaques and stent apposition in live patients. This chapter details the basic principles of intravascular optical coherence tomography (IV-OCT) in clinical practice. The system architecture and catheter structure consisting of an optical probe and a protective sheath are discussed in detail. Also, recent technology advances in IV-OCT are briefly introduced.

10.1 Introduction to OCT

Optical coherence tomography (OCT) is a high-resolution imaging modality that provides real-time cross-sectional images of tissue microstructures using the near-infrared light [1]. As OCT has common features with ultrasound imaging and microscopy in medical applications, it has been clinically adopted in ophthalmology, dermatology, and cardiology [2–4]. In most tissues, OCT imaging plays an important role in filling a gap between microscopy and ultrasound in comparison with resolution and imaging depth as shown in Fig. 10.1 [5]. Microscopy performs very high-resolution (~1 μm) imaging of en face tissue plane, but imaging depth in biological tissues is limited up to only a few hundred micrometers due to the signal attenuation from large optical scattering. The resolution of medical ultrasound imaging varies 0.1–1 mm depending on the sound wave frequency. It is, however, possible to see internal organs even if the imaging depth is limited to only millimeter ranges at high frequencies of ultrasound waves [6].

Compared with ultrasound imaging, OCT has the same operation principle, echo signal detection, but utilizes infrared light instead of ultrasound. In general, imaging is performed by measuring the magnitude and time delay of backscattered or backreflected signal from internal biological tissues. As a sound wave travels at 340 m/s in air, the echo signal can be measured with a time resolution of ~100 ns, which is within the limits of the electronic detection process. However, it is impossible to electrically measure echoes of backscattered light due to the light speed of 3×10^8 m/s in air, and optical interferometric techniques were then proposed [7–9]. Optical interferometers are widely used in science and engineering to measure small displacements and spatial irregularities by measuring interference patterns. To achieve microscale resolutions of the optical sectioning ability, low-coherence interferometry, using the short

J. Ha
Department of Optical Engineering, Sejong University, Seoul, South Korea
e-mail: jinyong.ha@gmail.com

M.-K. Hong (ed.), *Coronary Imaging and Physiology*,
https://doi.org/10.1007/978-981-10-2787-1_10

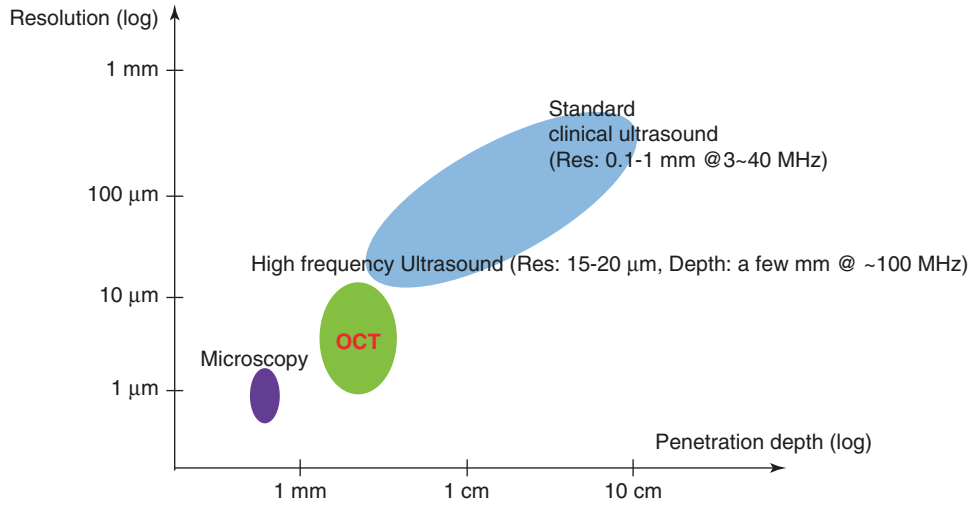

Fig. 10.1 Image resolution and penetration depth for OCT, microscopy, and ultrasound. OCT plays a role in filling a gap between microscopy and ultrasound in medical imaging. The image resolution in OCT is about 1–15 µm and the imaging depth is limited to 2–3 mm. Microscopy performs very high-resolution (~1 µm) imaging of en face tissue plane, but the imaging depth in biological tissues is limited up to only a few hundred micrometers due to the signal attenuation from large optical scattering. The resolution of medical ultrasound imaging varies 0.1–1 mm depending on the sound wave frequency, but it is possible to see internal organs even if imaging depth is limited to only millimeter ranges at high frequencies of ultrasound waves

coherence length of a broadband light source, is required. Low-coherence interferometry used in OCT is a unique solution to measure the echo signal of backscattered light with a very high signal-to-noise ratio, which is termed system sensitivity. The incident beam of light source is divided into a reference beam reflected from a mirror and a sample beam illuminated on biological tissues, and the sum of two beams is directed to a photodetector that measures the intensity of the combined signals [10].

10.1.1 Time Domain OCT and Frequency Domain OCT

OCT systems mainly consist of a light source, a coupler- or a circulator-based interferometer, and a photodetector. OCT is categorized into time domain OCT (TD-OCT) and frequency domain OCT (FD-OCT) as illustrated in Fig. 10.2 [11, 12]. TD-OCT employs a broadband light source such as a superluminescent diode and a scanning reference arm. The path length difference between the sample and reference arms of the interferometer is modulated by scanning a reference path length. The envelope of interference fringes is then extracted as a function of time, which means that image data is finally generated in a time domain. A single travel of the reference mirror creates a depth profile or an A-scan. Development of the high-speed scanning delay line of the reference arm allows OCT imaging speeds of several thousand axial profiles per second and video frame rate [13, 14]. FD-OCT additionally requires a spectrometer as a photodetector or wavelength-swept laser as light source without scanning a reference length. The former case is referred to as spectral domain OCT (SD-OCT), whereas the latter is termed swept-source OCT (SS-OCT) or alternatively optical frequency domain imaging (OFDI) [15–19]. SS-OCT has the advantages of easy implementation of polarization diverse detection as well as large depth range over SD-OCT. In the case of SS-OCT, a narrow instantaneous linewidth over a broad spectral range is tuned in wavelength as a function of time, and all echo signals from different depths are measured simultaneously. Thus, system sensitivity and imaging speeds can be dramatically improved [11, 19].

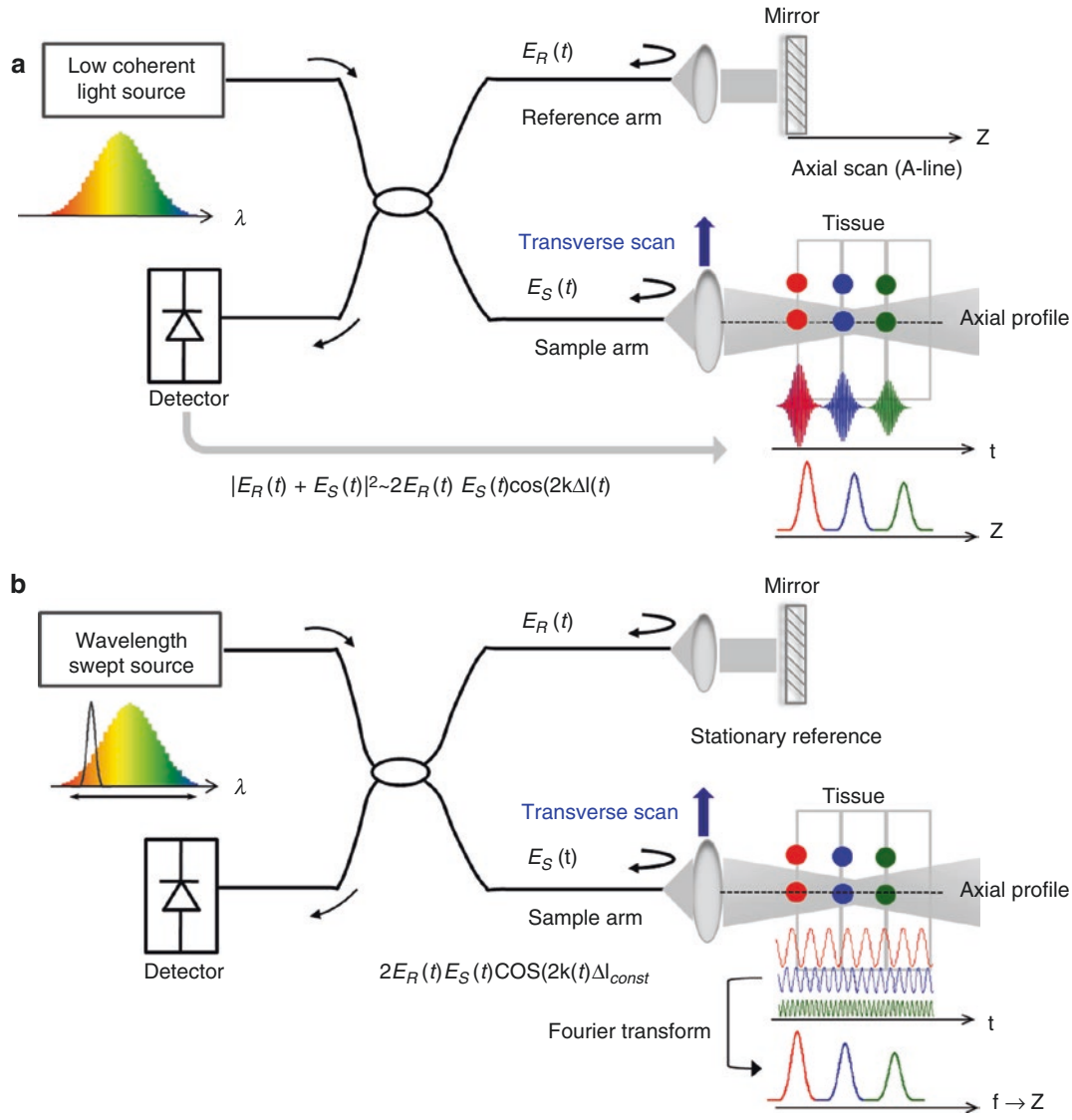

Fig. 10.2 Comparison between TD-OCT and FD-OCT. (**a**) Time domain optical coherence tomography (TD-OCT) system configuration consisting of a low-coherent light source, an interferometer, and a photodetector. To generate axial profiles, the reference arm is scanned as a function of time. (**b**) Frequency domain OCT (FD-OCT) system configuration. A wavelength-swept source is utilized and the reference arm is stationary. Interferometric patterns are measured as a function of wavelength and time, rather than as a function of time alone. The delay of echo signals from different positions in tissue results in different frequency modulations which are measured by Fourier transform

10.2 Intravascular OCT System

Intravascular OCT (IV-OCT) is a catheter-based imaging modality using a fiber-optic probe (Fig. 10.3). In general, in vivo intracoronary imaging is challenging because a suitable OCT catheter and contrast agent flushing protocols to remove blood need to be developed. IV-OCT additionally requires a catheter system that is composed of a rotary junction and a catheter as shown in Fig. 10.4 [20, 21]. A rotary junction plays the important role of pulling back and

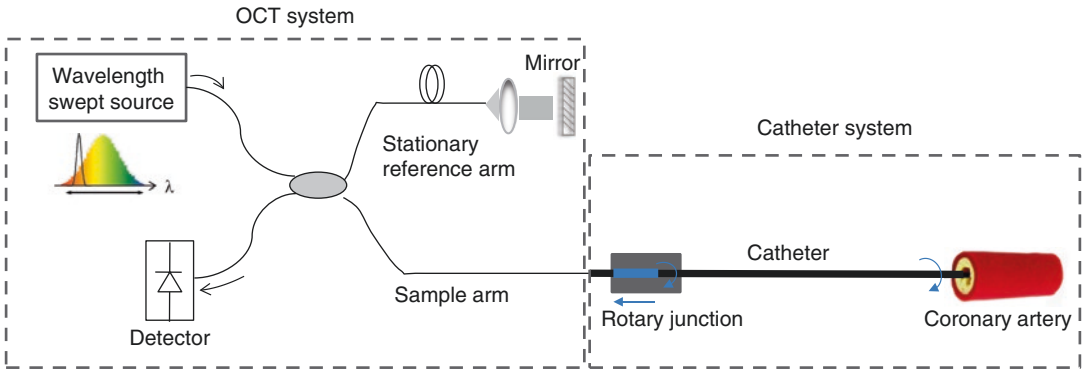

Fig. 10.3 Configuration of intravascular OCT. Intravascular OCT (IV-OCT) additionally requires a catheter system, which includes a rotary junction and a catheter. The rotary junction connects an IV-OCT platform to a catheter

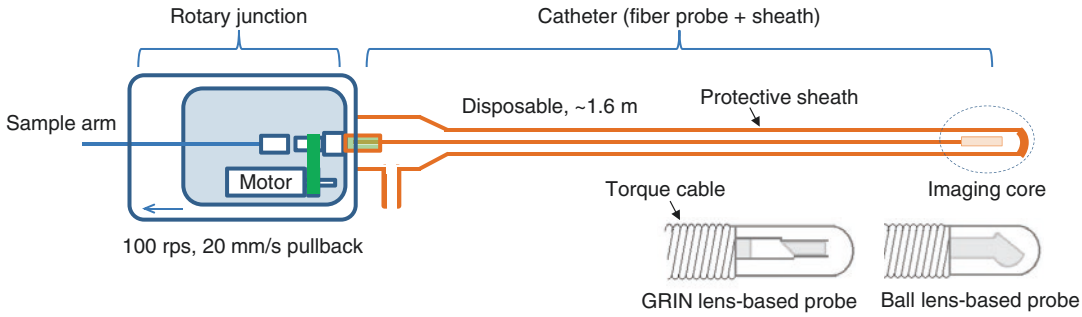

Fig. 10.4 Rotary junction and catheter structure. To create cross-sectional OCT images, a catheter needs to be rotated and pulled back by a rotary junction. The rotary junction also couples OCT light from the IV-OCT system to the fiber-optic probe in the protective sheath. To focus light beam, a GRIN lens or a polished ball lens is utilized. To provide the stable torque transmission from the proximal end to the distal tip of a fiber probe, the fiber probe is inserted into a hollow torque cable and fixed

rotating a catheter as well as optically connecting an OCT system console with a catheter. A catheter consists of an optical probe and a protective sheath. An optical probe is composed of a single mode fiber, a small lens, and a hollow torque cable. The torque cable has multiple threads and layers to accurately transmit the proximal end rotation to the distal tip of a fiber probe in curved environments. As a rotating optical fiber is prone to fragility, it is inserted into a torque cable and fixed. To focus light on the vessel, an angle-polished ball lens or a gradient index (GRIN) lens is utilized. An inserted catheter is rotated to create two-dimensional cross-sectional images of coronary artery while it is pulled back to generate multiple frames (Fig. 10.5). IV-OCT creates original rectangular OCT images that are converted from polar to Cartesian coordinates for display as shown in Fig. 10.6. To examine the coronary artery by IV-OCT, blood in the artery must be removed to avoid massive optical scattering and attenuation by red blood cells. The first catheter-based imaging of a human artery ex vivo was conducted by Tearney et al. [22, 23]. This study reported that OCT images were capable of differentiating the intima, media, and adventitia of the artery. The first in vivo IV-OCT imaging in human patients was conducted by Jang et al. who demonstrated a comparison of OCT with IVUS images of tissue prolapse in a stent [24].

The first commercial IV-OCT product was the M2 OCT system (LightLab Imaging, Inc., Westford, MA, USA, now part of St. Jude Medical, Inc.) with regulatory approval in Europe and Japan in 2004, and the M3 system was launched 3 years later in Japan. Since both M2

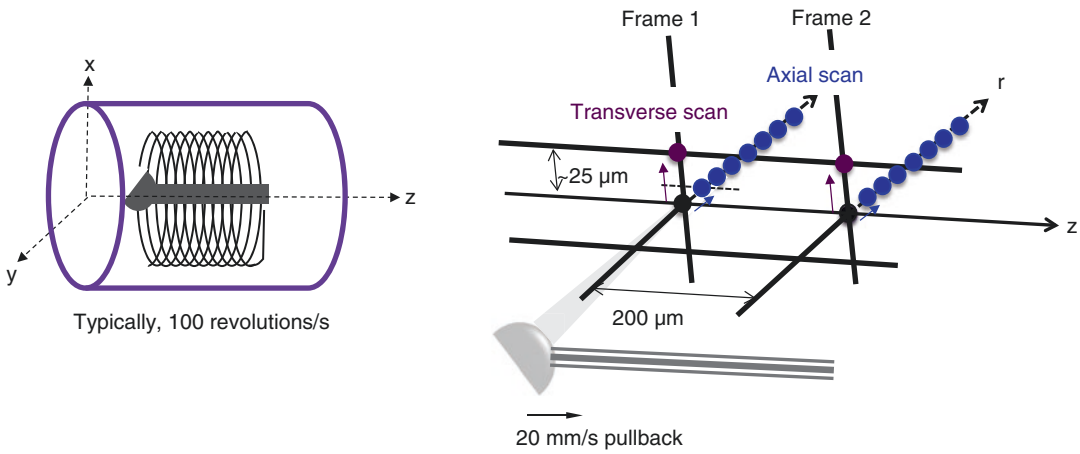

Fig. 10.5 Image data acquisition by helical scanning. Image data in IV-OCT are acquired by helical scanning of a catheter. This helical scanning consists of transverse scanning and pullback motion

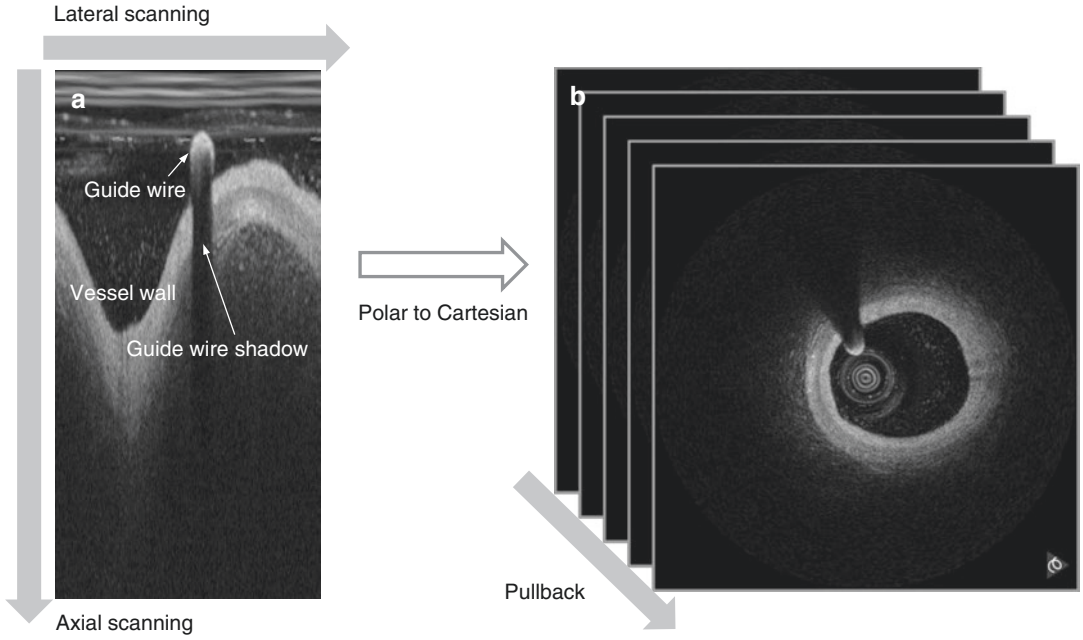

Fig. 10.6 Converting image in polar to Cartesian coordinate. IV-OCT images are generated by axial, lateral scannings and pullback motion. The original polar OCT images are transformed into Cartesian coordinates. (**a**) Rectangular OCT image in the polar domain naturally generated by IV-OCT. (**b**) Cross-sectional OCT image converted to Cartesian domain for visualization of coronary artery

and M3 systems were based on TD-OCT technology, the imaging speeds were limited (frame rate, 15.6/s for the M2 vs. 20/s for the M3, and pullback speed, 3.0 mm/s vs. 2.0 mm/s) [25, 26]. The balloon occlusion with lactated Ringer's solution or normal flushing was performed from proximal location to the lesion during the OCT imaging. Dramatic advancements in the wavelength-swept source in FD-OCT enabled much faster frame rates (100 frames/s) and pullback speeds (5–20 mm/s), resulting in non-occlusive OCT imaging with flushing of viscous

Table 10.1 Comparison of TD-OCT and FD-OCT

Imaging method	TD-OCT	FD-OCT
Axial resolution	15 μm	10–15 μm
Lateral resolution	90 μm	20–40 μm
Catheter profile	Maximum outer diameter of 0.019″	2.4-F to 3.2-F
Frame rate	16–20 frames/s (typ. 15.4 frames/s)	100–160 frames/s
Pullback speed	0.5–2 mm/s for occlusion 2–4 mm/s for non-occlusion	10–40 mm/s (typ. 20 mm/s)
Balloon occlusion	Highly recommended	Not required

contrast [4, 27]. The commercial version of FD-OCT, a Dragonfly imaging catheter and C7-XR OCT system (St. Jude Medical/LightLab Imaging, Westford, MA, USA), was launched with the world's first regulatory approval in 2010 [26]. The feasibility and safety of the Terumo OFDI system allowing 160 frames/s were evaluated in human patients in 2011 [28], and the first product of a LUNAWAVE OFDI system (Terumo Corporation, Tokyo, Japan) was then launched in more than 30 countries in Europe in 2013. The main specifications of TD-OCT and FD-OCT systems are summarized in Table 10.1 [4, 26, 28].

10.3 Image Quality of OCT

Since image quality is determined by imaging modality resolution, developing a high-resolution optical imaging system has been one of main research topics, involving high-speed and penetration depth imaging modalities. The image resolution of OCT is divided into axial resolution and lateral or transverse resolution. The axial resolution is the smallest distance between two objects that can be resolved along the axis of the incident beam. It is independent of the lens design and proportionally dependent on the center wavelength of light source and inversely proportional to the source bandwidth [29]. The lateral resolution in OCT imaging is the minimum resolvable distance between two objects which lie perpendicular to the OCT beam at the same depth position. It is mainly dependent on the focusing lens in the imaging core [30]. Another important parameter to determine the image quality is the depth of focus (DOF). DOF is twice the Rayleigh range, defined as the axial distance from the position of the minimum spot size (d) to the position of $\sqrt{2}d$. A trade-off exists between lateral resolution and DOF. Thus, increasing the lateral resolution to acquire better image quality results in decreasing the DOF. Since the relative position of a catheter from the vessel wall significantly varies during IV-OCT imaging, great variations of the lateral resolution induce distortion of images. The axial resolution for IV-OCT is typically ~10 μm at a center wavelength (~1300 nm) in the light source, and the lateral resolution is between 20 and 40 μm and the DOF is ~1.3 mm [31, 32].

10.3.1 Image Distortion in IV-OCT

Image artifacts in IV-OCT are mainly caused by catheter motion and cardiac dynamics. To create OCT cross-sectional images of vessels, a catheter is inserted into the coronary artery and rotated with an automatic pullback. Here, the torque applied at the proximal end of the catheter is not evenly transmitted to the distal imaging core, and thus the catheter is nonuniformly rotated since a catheter is placed through tortuous vessels or a crimped imaging sheath or a tight hemostatic value. This distortion is referred to as nonuniform rotational distortion, which also occurs in IVUS imaging [32]. Cardiac dynamics causes image distortion. During the cardiac cycle, heart motion directly affects the catheter motion in both the radial and longitudinal direction as shown in Fig. 10.7 [33, 34].

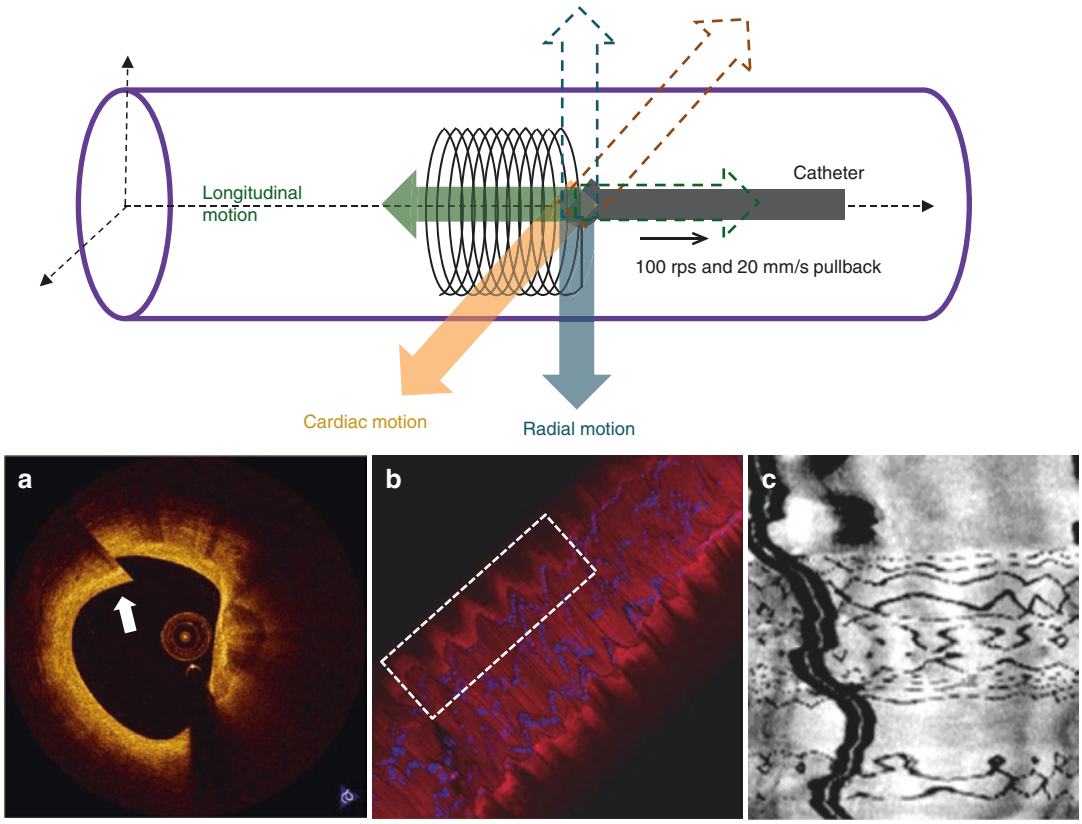

Fig. 10.7 Representative motion artifacts caused by cardiac motion. A catheter is significantly fluctuated in the coronary artery due to cardiac dynamics. Cardiac motion mainly generates the probe motion in the radial and longitudinal directions. During the cardiac cycle, the probe oscillates in both directions. (**a**) Cross-sectional view of coronary artery, (**b**) longitudinal cutaway view of the stented vessel caused by the radial motion artifact and (**c**) unfolded longitudinal view of the stented vessel due to the longitudinal motion artifact

As a result, an axial discontinuity in the cross-sectional image of coronary artery may appear at the transition region between the first and the last A-scan, and the repeated images of cross-sectional coronary artery can be generated by the longitudinal motion of a catheter that is pulled back and forth. In addition, there is also image distortion by saturation due to high optical backscattering, shadowing effect caused by blood inside of a catheter or stent struts, and suboptimal flushing [32].

10.4 Advances in IV-OCT Technology

Imaging speed, resolution, and penetration depth are most importantly considered when the performance of imaging modalities is evaluated. High-speed imaging may provide motion-artifact-free images and reduce the contrast flush volume. Recently, an ECG-triggered high-speed OCT system demonstrated a cardiac motion-free imaging at a rate of 500 frames/s and a pullback speed

of 100 mm/s, and the in vivo imaging experiment was conducted in a beating swine heart [35]. It was also reported that micro-OCT (μOCT) with enhanced lateral resolution of 1 μm proved an ability to observe cells, extracellular components, and endothelial coverage in situ although a μOCT catheter needs to be developed [36]. However, it may be difficult to improve penetration depth in tissue without increasing the center wavelength of light source, which decreases the axial resolution.

There has been a great deal of interest in identifying high-risk plaques by characterizing tissue components. Polarization-sensitive OCT (PS-OCT) is a functional extension and provides the property of tissue birefringence which may be associated with collagen and smooth muscle cell content [37, 38]. Recently, an in vivo human pilot study demonstrated the feasibility and robustness of intravascular PS-OCT by achieving improved tissue characterization such as plaque rupture [39, 40]. For other light-based approaches to detecting high-risk plaques, multimodality OCT combined with near-infrared fluorescence (NIRF) or near-infrared autofluorescence (NIRAF) has been demonstrated. Multimodality IV-OCT and NIRF imaging system accurately identified lipid-rich inflamed plaques using a FDA-approved indocyanine green (ICG) in rabbit models [41]. A first-in-human IV-OCT and NIRAF study was conducted with a 2.6-F coronary catheter. This study showed that an elevated NIRAF signal was focally associated with a high-risk morphological phenotype as determined by IV-OCT [42]. It was recently noted that the most advanced IVUS-OCT system at a rate of 72 frames/s was successfully demonstrated in a rabbit artery in vivo. The accurate registration between IVUS and OCT data sets showed great potential to accelerate the clinical adoption for accurate identification of vulnerable plaques in humans [43].

10.5 Summary

IV-OCT has a light-based imaging modality using an ultrathin catheter. Development of the high-speed imaging technology based on FD-OCT has enabled real-time non-occlusive coronary artery imaging. As IV-OCT has a great potential for further understanding and treatment for atherosclerotic coronary artery disease, new technologies will be constantly developed and revolutionized by taking multidisciplinary approaches.

References

1. Huang D, Swanson EA, Lin CP, Schuman JS, Stinson WG, Chang W, et al. Optical coherence tomography. Science. 1991;254(5035):1178–81.
2. Fercher AF, Hitzenberger CK, Drexler W, Kamp G, Sattmann H. In-vivo optical coherence tomography. Am J Ophthalmol. 1993;116(1):113–5.
3. Gladkova ND, Petrova GA, Nikulin NK, Radenska-Lopovok SG, Snopova LB, Chumakov YP, et al. In vivo optical coherence tomography imaging of human skin: norm and pathology. Skin Res Technol. 2000;6(1):6–16.
4. Tearney GJ, Waxman S, Shishkov M, Vakoc BJ, Suter MJ, Freilich MI, et al. Three-dimensional coronary artery microscopy by intracoronary optical frequency domain imaging. JACC Cardiovasc Imaging. 2008;1(6):752–61.
5. Drexler W, Fujimoto JG. Optical coherence tomography : technology and applications. Berlin: Springer; 2008. xxix, 1346 p.
6. Szabo TL. Diagnostic ultrasound imaging: inside out. Burlington: Elsevier; 2004.
7. Beaud P, Schutz J, Hodel W, Weber HP, Gilgen HH, Salathe RP. Optical reflectometry with micrometer resolution for the investigation of integrated optical-devices. IEEE J Quantum Electron. 1989;25(4):755–9.
8. Takada K, Yokohama I, Chida K, Noda J. New measurement system for fault location in optical waveguide devices based on an interferometric-technique. Appl Opt. 1987;26(9):1603–6.
9. Youngquist RC, Carr S, Davies DEN. Optical coherence-domain Reflectometry—a new optical evaluation technique. Opt Lett. 1987;12(3):158–60.
10. Huang D, Wang J, Lin CP, Puliafito CA, Fujimoto JG. Micron-resolution ranging of cornea anterior chamber by optical reflectometry. Lasers Surg Med. 1991;11(5):419–25.
11. Choma MA, Sarunic MV, Yang CH, Izatt JA. Sensitivity advantage of swept source and Fourier domain optical coherence tomography. Opt Express. 2003;11(18):2183–9.
12. Leitgeb R, Hitzenberger C, Fercher A. Performance of fourier domain vs. time domain optical coherence tomography. Opt Express. 2003;11(8):889–94.
13. Rollins AM, Kulkarni MD, Yazdanfar S, Ungarunyawee R, Izatt JA. In vivo video rate optical coherence tomography. Opt Express. 1998;3(6):219–29.

14. Tearney GJ, Bouma BE, Fujimoto JG. High-speed phase- and group-delay scanning with a grating-based phase control delay line. Opt Lett. 1997;22(23):1811–3.
15. Chinn SR, Swanson EA, Fujimoto JG. Optical coherence tomography using a frequency-tunable optical source. Opt Lett. 1997;22(5):340–2.
16. Fercher AF, Hitzenberger CK, Kamp G, Elzaiat SY. Measurement of intraocular distances by backscattering spectral interferometry. Opt Commun. 1995;117(1–2):43–8.
17. Golubovic B, Bouma BE, Tearney GJ, Fujimoto JG. Optical frequency-domain reflectometry using rapid wavelength tuning of a Cr4+:forsterite laser. Opt Lett. 1997;22(22):1704–6.
18. Yun SH, Tearney GJ, Bouma BE, Park BH, de Boer JF. High-speed spectral-domain optical coherence tomography at 1.3 mu m wavelength. Opt Express. 2003;11(26):3598–604.
19. Yun SH, Tearney GJ, de Boer JF, Iftimia N, Bouma BE. High-speed optical frequency-domain imaging. Opt Express. 2003;11(22):2953–63.
20. Tearney GJ, Boppart SA, Bouma BE, Brezinski ME, Weissman NJ, Southern JF, et al. Scanning single-mode fiber optic catheter-endoscope for optical coherence tomography. Opt Lett. 1996;21(7):543–5.
21. Yaqoob Z, Wu JG, McDowell EJ, Heng X, Yang CH. Methods and application areas of endoscopic optical coherence tomography. J Biomed Opt. 2006;11(6):063001.
22. Tearney GJ, Brezinski ME, Boppart SA, Bouma BE, Weissman N, Southern JF, et al. Catheter-based optical imaging of a human coronary artery. Circulation. 1996;94(11):3013.
23. Tearney GJ, Jang IK, Kang DH, Aretz HT, Houser SL, Brady TJ, et al. Optical coherence tomography of human coronary arteries: a new imaging modality to visualize different components of plaques. J Am Coll Cardiol. 2000;35(2):52a–3a.
24. Jang IK, Tearney G, Bouma B. Visualization of tissue prolapse between coronary stent struts by optical coherence tomography—comparison with intravascular ultrasound. Circulation. 2001;104(22):2754.
25. Inami S, Wang Z, Ming-Juan Z, Takano M, Mizuno K. Current status of optical coherence tomography. Cardiovasc Interv Ther. 2011;26(3):177–85.
26. Terashima M, Kaneda H, Suzuki T. The role of optical coherence tomography in coronary intervention. Korean J Intern Med. 2012;27(1):1–12.
27. Yun SH, Tearney GJ, Vakoc BJ, Shishkov M, Oh WY, Desjardins AE, et al. Comprehensive volumetric optical microscopy in vivo. Nat Med. 2006;12(12):1429–33.
28. Okamura T, Onuma Y, Garcia-Garcia HM, van Geuns RJ, Wykrzykowska JJ, Schultz C, et al. First-in-man evaluation of intravascular optical frequency domain imaging (OFDI) of Terumo: a comparison with intravascular ultrasound and quantitative coronary angiography. EuroIntervention. 2011;6(9):1037–45.
29. Swanson EA, Huang D, Hee MR, Fujimoto JG, Lin CP, Puliafito CA. High-speed optical coherence domain reflectometry. Opt Lett. 1992;17(2):151–3.
30. Saleh BEA, Teich MC. Fundamentals of photonics. 2nd ed. Hoboken: Wiley; 2007. xix, 1175 p.
31. Lowe HC, Narula J, Fujimoto JG, Jang IK. Intracoronary optical diagnostics current status, limitations, and potential. JACC Cardiovasc Interv. 2011;4(12):1257–70.
32. Tearney GJ, Regar E, Akasaka T, Adriaenssens T, Barlis P, Bezerra HG, et al. Consensus standards for acquisition, measurement, and reporting of intravascular optical coherence tomography studies: a report from the international working group for intravascular optical coherence tomography standardization and validation. J Am Coll Cardiol. 2012;59(12):1058–72.
33. Ha JY, Shishkov M, Colice M, Oh WY, Yoo H, Liu L, et al. Compensation of motion artifacts in catheter-based optical frequency domain imaging. Opt Express. 2010;18(11):11418–27.
34. Ha J, Yoo H, Tearney GJ, Bouma BE. Compensation of motion artifacts in intracoronary optical frequency domain imaging and optical coherence tomography. Int J Cardiovasc Imaging. 2012;28(6):1299–304.
35. Jang SJ, Park HS, Song JW, Kim TS, Cho HS, Kim S, et al. ECG-triggered, single cardiac cycle, high-speed, 3D, intracoronary OCT. JACC Cardiovasc Imaging. 2016;9(5):623–5.
36. Liu LB, Gardecki JA, Nadkarni SK, Toussaint JD, Yagi Y, Bouma BE, et al. Imaging the subcellular structure of human coronary atherosclerosis using micro-optical coherence tomography. Nat Med. 2011;17(8):1010–U132.
37. Kuo WC, Chou NK, Chou C, Lai CM, Huang HJ, Wang SS, et al. Polarization-sensitive optical coherence tomography for imaging human atherosclerosis. Appl Opt. 2007;46(13):2520–7.
38. Nadkarni SK, Pierce MC, Park BH, de Boer JF, Whittaker P, Bouma BE, et al. Measurement of collagen and smooth muscle cell content in atherosclerotic plaques using polarization-sensitive optical coherence tomography. J Am Coll Cardiol. 2007;49(13):1474–81.
39. van der Sijde JN, Karanasos A, Villiger M, Bouma BE, Regar E. First-in-man assessment of plaque rupture by polarization-sensitive optical frequency domain imaging in vivo. Eur Heart J. 2016;37(24):1932.
40. Villiger M, Karanasos A, Ren J, Lippok N, Shishkov M, van Soest G, et al., editors. Intravascular polarization sensitive optical coherence tomography in human patients. Conference on Lasers and Electro-Optics. San Jose: Optical Society of America; 2016.
41. Lee S, Lee MW, Cho HS, Song JW, Nam HS, Oh DJ, et al. Fully integrated high-speed intravascular optical coherence tomography/near-infrared fluorescence structural/molecular imaging in vivo using a clinically available near-infrared fluorescence-emitting indocyanine green to detect inflamed lipid-rich atheromata in coronary-sized vessels. Circ Cardiovasc Interv. 2014;7(4):560–9.

42. Ughi GJ, Wang H, Gerbaud E, Gardecki JA, Fard AM, Hamidi E, et al. Clinical characterization of coronary atherosclerosis with dual-modality OCT and near-infrared autofluorescence imaging. JACC Cardiovasc Imaging. 2016;9(11):1304–14.

43. Li J, Ma T, Mohar D, Steward E, Yu M, Piao Z, et al. Ultrafast optical-ultrasonic system and miniaturized catheter for imaging and characterizing atherosclerotic plaques in vivo. Sci Rep. 2015;5:18406.